Journal of the Korean Ceramic Society (2024) 61:411–418
https://doi.org/10.1007/s43207-023-00343-z

ORIGINAL ARTICLE

Magnetic, thermoelectric properties and magnetocaloric effect of $Pr_{0.7}Ba_{0.3}MnO_3$ perovskite: experimental, DFT calculation and Monte Carlo simulations

R. Masrour[1] · G. Kadim[1] · M. Ellouze[2]

Received: 8 July 2023 / Revised: 2 November 2023 / Accepted: 7 November 2023 / Published online: 18 December 2023

Abstract
The magnetic, electronic, structural, thermoelectric properties and magnetocaloric effect of $Pr_{0.75}Ba_{0.25}MnO_3$ perovskite using, experimental, DFT calculation and Monte Carlo simulations were investigated. The ground state has half-metallic character. Our calculations also show that the $Pr_{0.75}Ba_{0.25}MnO_3$ has a ferromagnetic behavior. $Pr_{0.75}Ba_{0.25}MnO_3$ exhibits p-type behavior with dominant holes as the primary carriers, as indicated by its thermoelectric properties. This system exhibits a ferromagnetic–Paramagnetic transition. We have successfully obtained several properties, including magnetization, specific heat, variation of specific heat, magnetic entropy changes, relative cooling power, and the magnetic hysteresis cycle. For a magnetic field change of 5 T, the maximum value of the magnetic entropy change ($|\Delta S^{max}|$) was approximately 12 J/kg.K, while the relative cooling power (RCP) reached 126 J/kg. The promising potential of the present system for magnetic refrigeration is evident due to its relatively large values of $|\Delta S^{max}|$ and RCP. Finally, the thermoelectric properties were given.

Keywords MCE · RCP and magnetic entropy changes · Hysteresis cycle and specific heat · Thermoelectric

1 Introduction

Manganite-based perovskites are attractive functional materials, because they possess a wide range of reported inclusion physical properties, such as the magnetocaloric effect and thermoelectric properties [1–6]. These physical properties make these materials intended for several applications [7–14]. Experimentally, the magnetic and structural properties of $Pr_{0.7}Ba_{0.2}Ca_{0.1}MnO_3$ were investigated [15]. A study was conducted to investigate the impact of compaction pressure on the enhancement of ferromagnetic properties in $La_{0.7}Ba_{0.3}MnO_3$ [16]. $Pr_{0.75}Sr_{0.25}MnO_3$ exhibited a semiconductor–metal transition [17]. $Pr_{0.75}Sr_{0.25}MnO_3$ has a half-metallic character with a huge band gap of 2.8 eV in the minority band [18]. This property of the half metals make them potential candidates for application in spintronic devises and magnetic sensors.

In the present work, we have prepared $Pr_{0.7}Ba_{0.3}MnO_3$ using solid-state reaction method (more detailed is given in Refs. [19, 20]. The structural and morphological of the prepared samples were investigated. Furthermore, the electronic and thermoelectric properties of $Pr_{0.75}Ba_{0.25}MnO_3$ are investigated using DFT calculation [21–26]. In addition, The Monte Carlo simulations (MCSs) calculations are used to shed light on the magnetic and magnetocaloric properties of $Pr_{0.75}Ba_{0.25}MnO_3$. The T dependence of the magnetization is given. The thermal specific heat, variation of heat specific, magnetic entropy changes, relative cooling power, and magnetic hysteresis cycle are obtained.

2 Model and simulations method

The Hamiltonian of this system

✉ R. Masrour
rachidmasrour@hotmail.com

[1] Laboratory of Solid Physics, Faculty of Sciences Dhar El Mahraz, Sidi Mohamed Ben Abdellah University, BP 1796 Fez, Morocco

[2] LMEEM, Faculty of Sciences of Sfax (FSS), University of Sfax, B. P.1171, 3000 Sfax, Tunisia

$$H = -J_1 \sum_{<i,j>} S_i S_j - J_2 \sum_{<<i,k>>} S_i S_k - J_3 \sum_{<<<i,l>>>} S_i S_l - J_4 \sum_{<<<<i,m>>>>} S_i S_m - h \sum_i S_i. \quad (1)$$

The J_1, J_2, J_3 and J_4 are the first, second, third, and fourth exchange interactions between Mn–Mn in $Pr_{0.75}Ba_{0.25}MnO_3$ with $S(Mn^{4+}) = 3/2$.

The obtained results by DFT were used to calculate the exchange interaction between the magnetic atoms, $J_1 = 15.3$, $J_2 = 12.3$, $J_3 = 12.1$, $J_4 = 9.5$ K. Magnetocaloric effect $Pr_{0.7}Ba_{0.3}MnO_3$ has been studied.

The magnetic and magnetocaloric properties of $Pr_{0.75}Ba_{0.25}MnO_3$ were investigated using Monte Carlo simulations (MCSs) in conjunction with the Metropolis algorithm. Equation (1) was employed for this purpose.

The magnetization of Mn^{4+} in this perovskite

$$M = \left\langle \frac{1}{N} \sum_i S_i \right\rangle \quad (2)$$

with $N = 2465$ spins.

The specific heat of this perovskite

$$C_P = \frac{\beta}{N^2} \left(\left\langle E^2 \right\rangle - \langle E \rangle^2 \right), \quad (3)$$

where $\beta = \frac{1}{k_B T}$.

The magnetic entropy changes

$$\Delta S(T,h) = \int_0^{h_{\max}} \left(\frac{\partial M}{\partial T} \right)_{h_i} dh. \quad (4)$$

The RCP

$$\mathrm{RCP} = \int_{T_1}^{T_2} \Delta S(T) dT. \quad (5)$$

3 Crystallographic structure and computational details

The structure de $Pr_{0.7}$ Ba $_{0.3}MnO_3$ dans le plan (b, c) and in [111] plane is presented in Figs. 1 and 2, respectively. The lattice parameters of our system are given in Table 1.

In Table 2, we have presented the crystallographic parameters $Pr_{0.7}$ $Ba_{0.3}MnO_3$, and n is percentage occupancy.

The numbers in parentheses represent the error and the results in braces are for the $Pr_{0.7}$ Ba $_{0.3}MnO_3$ compound.

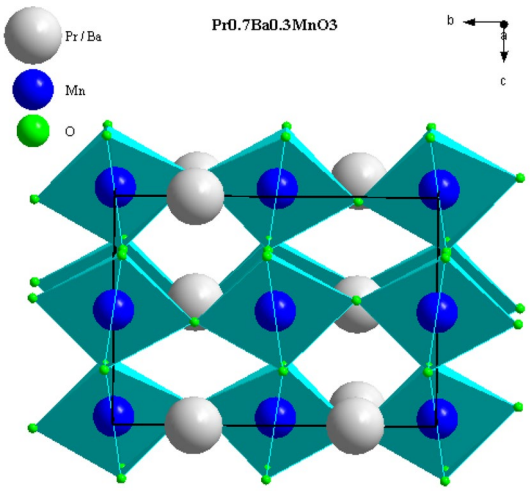

Fig. 1 Structure of $Pr_{0.75}Ba_{0.25}MnO_3$ (b, c) plane

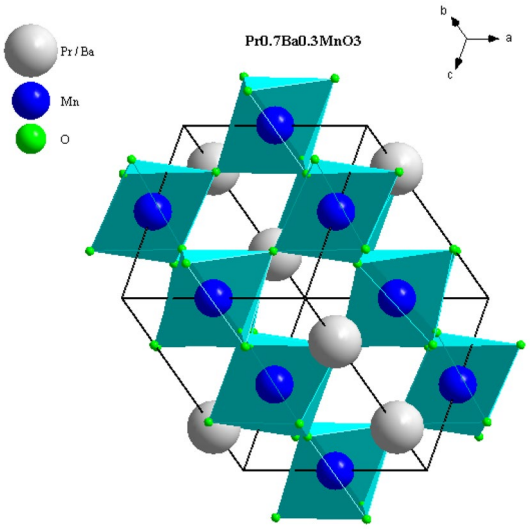

Fig. 2 Structure of $Pr_{0.7}Ba_{0.3}MnO_3$ in [111] plan

Table 1 Lattice parameters of $Pr_{0.7}Ba_{0.3}MO_3$ given by Refs. [19, 20]

Compound	a (Å)	b (Å)	c (Å)
$Pr_{0.7}Ba_{0.3}MnO_3$	5.4900	7.7578	5.5227

Table 2 Crystallographic parameters $Pr_{0.7}Ba_{0.3}MnO_3$, and n is percentage occupancy [20]

Atoms	Site	x	y	Z	n (%)
Pr/Ba	4c	0.0012 (1)	0.25	– 0.0022(1)	70/30
Mn	4b	0.0	0.0	0.5	100
O (1)	4c	0.5446 (5)	0.25	0.0506(1)	100
O (2)	8d	0.2489 (1)	0.0253 (7)	0.7613(3)	100

In this work, DFT calculations were perfumed using approximate XC functional GGA executed via operating the PBE method as implemented in the Wien2k package [27–32]. In the electronic properties part, we take a concentration of 0.25 instead of 0.3. To avoid supercells, which give us too many atoms in the structure and which can spoil the convergence of the calculation. A cut-off parameter is $R_{MT} \times K_{max} = 8$ and the Fourier expansion parameter $G_{max} = 12.0$. The transport properties of $Pr_{0.75}Ba_{0.25}MnO_3$ are obtained using the semi-classical Boltzmann theory as implemented in the BoltzTraP code [33]. Furthermore, in the BoltzTraP code, the semi-classical transport equations of Bloch–Boltzmann are solved in the constant relaxation time approximation [33]. The transport coefficients using the constant relaxation time approximation are $\tau = 10^{-14}$ s [34].

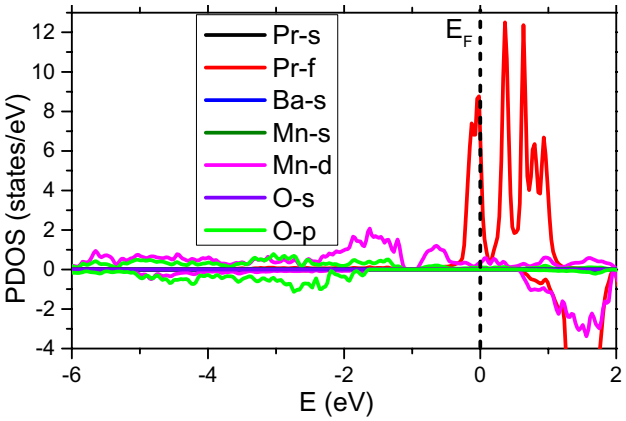

Fig. 4 Total PDOS of $Pr_{0.75}Ba_{0.25}MnO_3$ calculated using GGA approximation

4 Results and discussion

The spin-polarized total and partial electronic density of states (DOS) for $Pr_{0.75}Ba_{0.25}MnO_3$ are depicted in Figs. 3 and 4, respectively. The asymmetrical nature observed between the spin-up and spin-down DOS confirms the magnetic properties of the material. The magnetization is attributed to the transition metal Mn and the rare-earth element Pr. Specifically, the spin moment values are determined to be 1.89023 μ_B for Pr and 3.37955 μ_B for Mn. At the Fermi level (E_F), the majority band exhibits conducting behavior, while the minority band displays insulating characteristics. This configuration allows for 100% spin polarization and exhibits a half-metallicity feature, with a band gap of 2.274 eV in the minority band. This half-metallicity property positions $Pr_{0.75}Ba_{0.25}MnO_3$ as a promising candidate for applications in spintronic devices and magnetic sensors.

The partial DOS shows that Mn-3d and O-2p have an important electron density contribution in region [−6, −0.25 eV]. In the energy range of [−0.25, +2 eV], which encompasses the conduction band, the orbital hybridization is primarily influenced by the spin-up states of Pr-4f, Mn-3d, and O-2p orbitals. Within this range, an exchange splitting can be observed between the spin-down and spin-up partial states of Pr-4f and Mn-3d orbitals. This exchange splitting plays a significant role in contributing to the majority portion of the total spin magnetic moments of the unit cell in $Pr_{0.75}Ba_{0.25}MnO_3$ compound.

Figure 5 illustrates the relationship between magnetization and temperature (magnetization vs. temperature curve) and magnetic susceptibility vs. temperature for $Pr_{0.75}Ba_{0.25}MnO_3$. The data reveal a transition from a ferromagnetic phase to a paramagnetic phase, which occurs at a critical temperature (T_C) of 156 K. Our value is near to that given by Ref. [20] ($T_C = 164$ K), and this difference may be

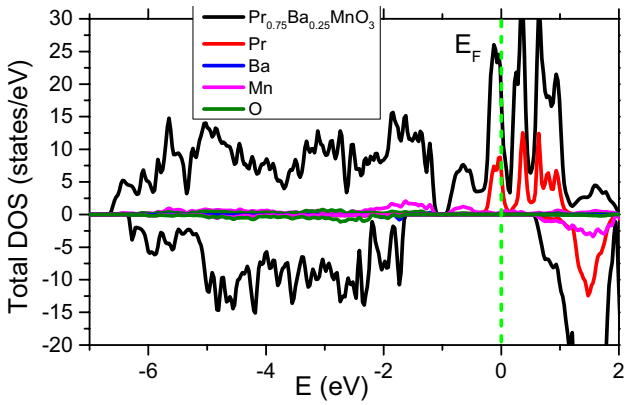

Fig. 3 Total DOS of $Pr_{0.75}Ba_{0.25}MnO_3$ Pr, Ba, Mn, and O atoms calculated using GGA approximation

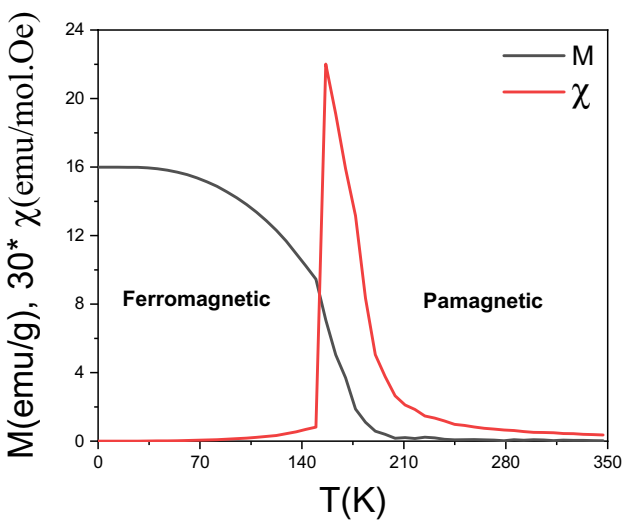

Fig. 5 The thermal magnetization and magnetic susceptibility of $Pr_{0.75}Ba_{0.25}MnO_3$

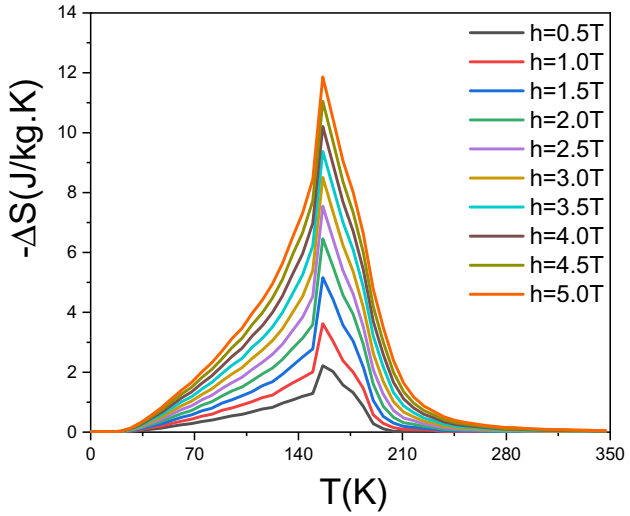

Fig. 6 The thermal entropy magnetic change of $Pr_{0.75}Ba_{0.25}MnO_3$ for several magnetic fields *h*

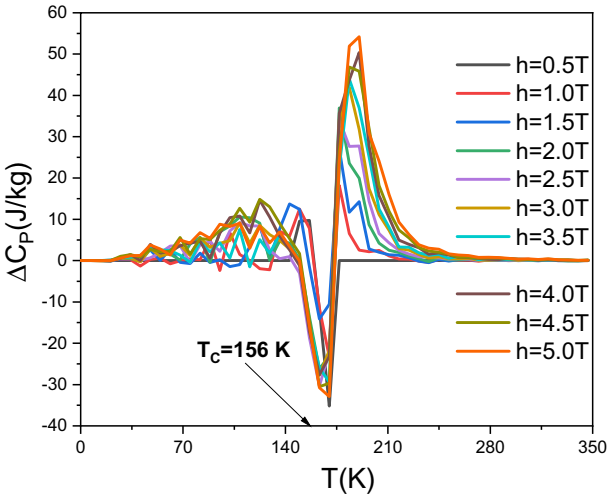

Fig. 8 The thermal specific heat changes and magnetic susceptibility of $Pr_{0.75}Ba_{0.25}MnO_3$

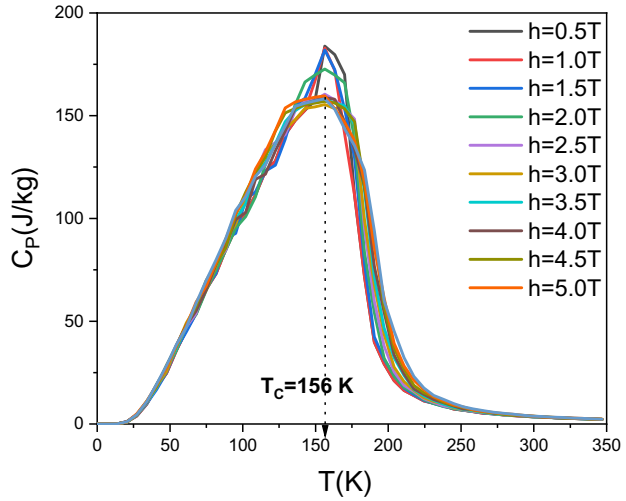

Fig. 7 The thermal specific heat of $Pr_{0.75}Ba_{0.25}MnO_3$

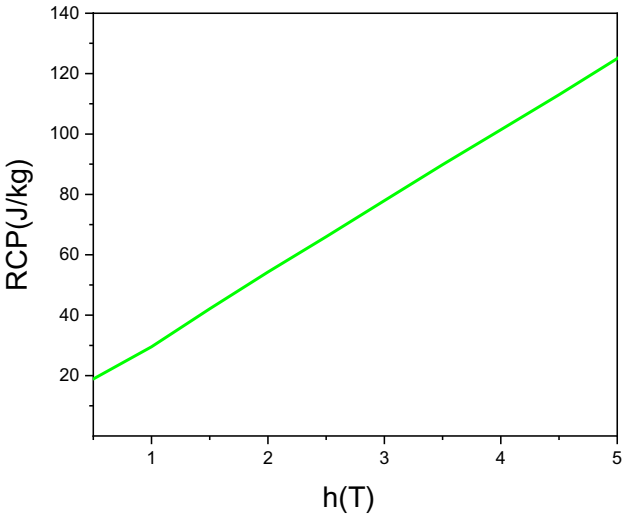

Fig. 9 The RCP vs. $h(T)$ of $Pr_{0.75}Ba_{0.25}MnO_3$ for T_C = 0.015 K and T_h = 350 K

due to the atoms that we did not consider in our Pr, Br, and O calculation, because they are not magnetic. The value of saturation magnetization is equal 16 emu/g. This value is near to that obtained by the experiment results [20].

The magnetic entropy changes are given in Fig. 6. The value of ΔS^{max} is situated at the $T_c = 156$ K. For $h = 5.0$ T, the value of ΔS^{max} is 12 and 2.46 J/kg.K for 0.5 T. ΔS vs. temperature was given in Ref. [35]. In previous work [15] for $Pr_{0.7}Ba_{0.2}Ca_{0.1}MnO_3$, they found that 2.2 J/kg.K for 5 T.

The variation of specific heat C_P vs. temperature is shown in Fig. 7. The maximum of C_P is situated at 156 K. As the magnetic field values increase, there is a decrease in the maximum value of the specific heat capacity (C_P). The large anomaly in the heat capacity of $DyAl_2$ was observed due mainly to spin reorientation from [100] to [111][36].

The C_P changes exhibit anomaly near to T_C due to the ferromagnetic–paramagnetic transition. The thermal specific heat changes strongly changes from the negative value to the positive one as temperature increases (Fig. 8).

The relative cooling power vs. magnetic field is given in Fig. 9. The value of RCP obtained by Ref. [15] is 261 J/kg for 5 T and in this work for $Pr_{0.7}Ba_{0.3}MnO_3$ is 126 J/kg for 5 T. The RCP vs. temperature is illustrated in Fig. 10. The RCP exhibits an anomalous around the $T_C = 156$ K. The relative cooling power (RCP) increases with increasing temperature until it reaches a saturation point for each value of

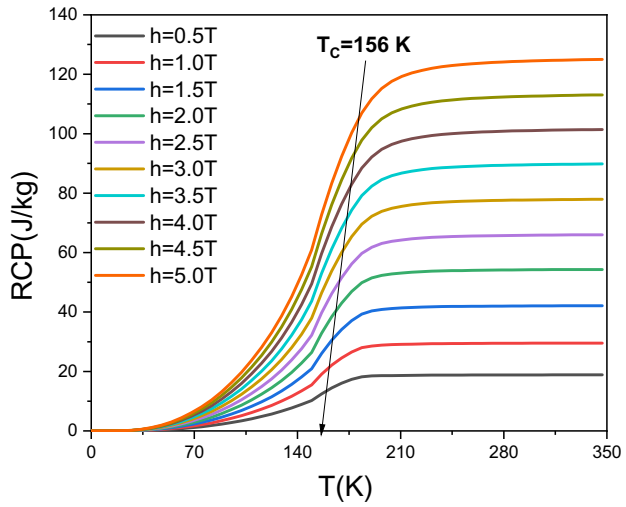

Fig. 10 The RCP vs. T(K) of $Pr_{0.75}Ba_{0.25}MnO_3$ for several magnetic field

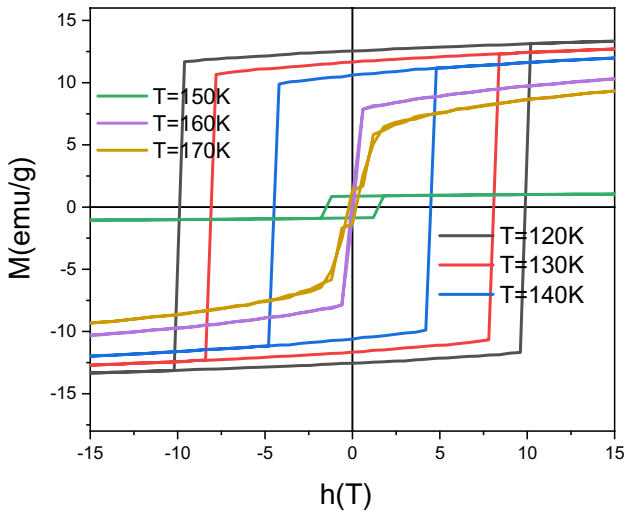

Fig. 11 The M(emu/g) vs. $h(T)$ of $Pr_{0.75}Ba_{0.25}MnO_3$ for several temperatures

the magnetic field (h). Regarding the effect of the magnetic field (h), RCP increases as the value of h increases, as shown in Fig. 8. The magnetization versus magnetic field (h) is depicted in Fig. 11 for three different temperatures: 150 K, 130 K, and 170 K. It can be observed that the remanent magnetization and coercive field decrease with increasing temperature. $Pr_{0.75}Ba_{0.25}MnO_3$ demonstrates a superparamagnetic behavior around the temperature T_C.

To provide a more accurate response, I would need the complete relation for calculating the Seebeck coefficient. Could you please provide the full relation or equation for calculating the Seebeck coefficient

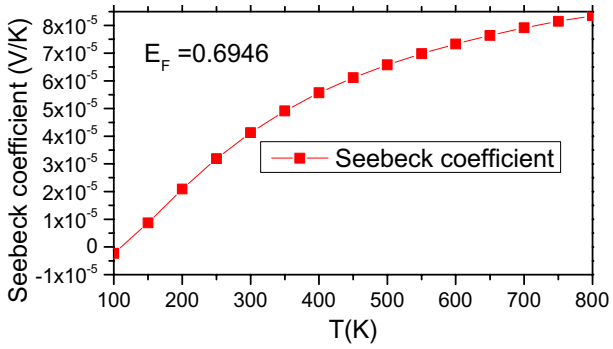

Fig. 12 Variation of Seebeck coefficient with temperature for $Pr_{0.75}Ba_{0.25}MnO_3$

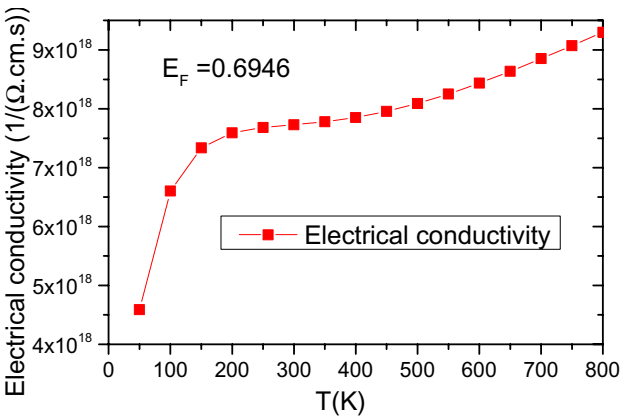

Fig. 13 Variation of electrical conductivity vs. T(K) for $Pr_{0.75}Ba_{0.25}MnO_3$

$$S = T\frac{8\pi^2 k_B^2 m^*}{3eh^2}\left(\frac{\pi}{3n}\right)^{2/3}; \tag{6}$$

so, n is charge carrier concentration, m^* is the effective mass, k_B is Boltzmann constant, $e = 1.67 \times 10^{-19}C$, and $h = 6.626 \times 10^{-26}$ k.g.m^2 sec^{-1} h.

Figure 12 illustrates the variation of the Seebeck coefficient (S) for $Pr_{0.75}Ba_{0.25}MnO_3$. The data reveal that the Seebeck coefficient increases as the temperature increases. At 800 K, it reaches a value of 8×10^{-15} V/K. The positive value of the Seebeck coefficient for $Pr_{0.75}Ba_{0.25}MnO_3$ indicates that the dominant charge carriers are holes. This positive Seebeck coefficient aligns with the p-type behavior exhibited by the material.

The electrical conductivity (σ) of $Pr_{0.75}Ba_{0.25}MnO_3$ is depicted in Fig. 13. It is generally observed that the electrical conductivity is directly proportional to the charge carrier concentration (n) and the mobility (μ). At 800 K, $Pr_{0.75}Ba_{0.25}MnO_3$ exhibits a high electrical conductivity with a value of $9.35.10^{18}\Omega^{-1}.m^{-1}.s^{-1}$. On the other hand, the thermal conductivity (κ) reflects a material's ability to conduct and transmit heat. Figure 14 displays the variation

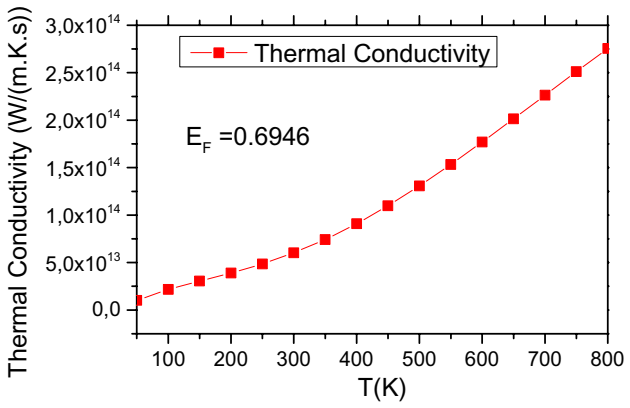

Fig. 14 Variation of electronic thermal conductivity κ_e/τ vs. T(K) for $Pr_{0.75}Ba_{0.25}MnO_3$

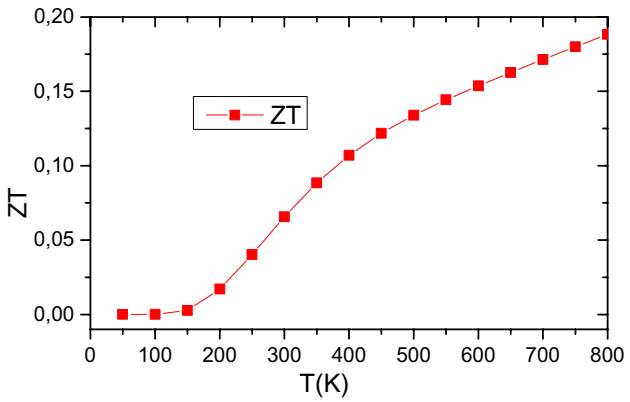

Fig. 15 Variation of figure of merit vs. T(K) for $Pr_{0.75}Ba_{0.25}MnO_3$

of thermal conductivity with temperature. As depicted, the thermal conductivity increases as the temperature rises. The maximum value of thermal conductivity observed in the figure is $2.75.10^{14} W.K^{-1}.m^{-1}.s^{-1}$.

The figure of merit ZT is calculated by the following relation:

$$\mathrm{ZT} = T\frac{S^2\sigma}{\kappa}, \tag{7}$$

with $k = k_l + k_e$, k_l defines the lattice thermal conductivity and *ke* denotes electronic thermal energy. The lattice component of thermal conductivity *kl* caused by the phonon scattering is not considered in our calculations. As an estimate of $Pr_{0.75}Ba_{0.25}MnO_3$ efficiency.

In Fig. 15, the variation of the ZT coefficient for $Pr_{0.75}Ba_{0.25}MnO_3$ is displayed. The plot demonstrates that the ZT value increases as the temperature rises. The highest ZT value obtained is 0.19 at 800 K. Given that the thermal conductivity due to phonons is included in the calculations, this value of 0.19 is considered reasonable. It suggests that the thermal conductivity contribution from the lattice component (*kl*) is significant.

5 Conclusions

In our study, we employed a combination of experimental techniques, density functional theory (DFT), and Monte Carlo simulations (MCSs) to investigate the electronic, thermoelectric, magnetic properties, and magnetocaloric effect of the $Pr_{0.75}Ba_{0.25}MnO_3$ perovskite system. One of the key findings is that the $Pr_{0.75}Ba_{0.25}MnO_3$ perovskite exhibits a half-metallic character, with a band gap of 2.274 eV in the minority band. This indicates that it can selectively conduct one spin direction while behaving as an insulator for the opposite spin direction. We also determined the transition temperature, which was found to be in close agreement with experimental results, validating the accuracy of our approach. By analyzing the magnetization as a function of temperature, we were able to deduce the magnetic entropy change (ΔS). It was observed that ΔSmax increases with the applied magnetic field (h). This suggests that the ferromagnetic order in the samples exhibits long-range characteristics. Furthermore, we observed a significant magnetocaloric effect at a magnetic field of 5 T, accompanied by large values of ΔS_{max} and relative cooling power (RCP). These findings indicate that the $Pr_{0.75}Ba_{0.25}MnO_3$ perovskite system holds promise for magnetic refrigeration applications. In terms of thermoelectric properties, our theoretical investigation revealed that $Pr_{0.75}Ba_{0.25}MnO_3$ exhibits p-type behavior, with holes being the dominant charge carriers. This characterization of the material's electronic behavior provides valuable insights into its thermoelectric performance. Overall, the combination of the observed large magnetocaloric effect, relatively high RCP, and high magnetization makes the $Pr_{0.75}Ba_{0.25}MnO_3$ perovskite system a promising candidate for applications in magnetic refrigeration and spintronics.

Funding No funding.

Data availability Not applicable.

Declarations

Conflict of interest No conflict interests.

References

1. G. Kadim, R. Masrour, A. Jabar, E.K. Hlil, Room-temperature large magnetocaloric, electronic and magnetic properties in $La_{0.75}Sr_{0.25}MnO_3$ manganite: Ab initio calculations and Monte Carlo simulations. Phys. A: Stat. Mech. Appl. **573**, 125936 (2021)
2. G. Kadim, R. Masrour, A. Jabar, E.K. Hlil, First principal calculation and Monte Carlo simulations of the magnetocaloric effect, electronic and magnetic properties in perovskite oxide $Pr_{0.65}Sr_{0.35}MnO_3$. IOP Conf. Ser.: Mater. Sci. Eng. **1160**(1), 012010 (2021)
3. Y. Xu, J. Dhainaut, J.P. Dacquin, J.F. Lamonier, H. Zhang, S. Royer, On the role of cationic defects over the surface reactivity of manganite-based perovskites for low temperature catalytic oxidation of formaldehyde. Appl. Catal. B Environ. **342**, 123400 (2023)
4. X. Yang, T. Wei, B. Chi, J. Pu, J. Li, Lanthanum manganite-based perovskite as a catalyst for co-production of ethylene and hydrogen by ethane dehydrogenation. J. Catal. **377**, 629–637 (2019)
5. S. Taran, B.K. Chaudhuri, S. Chatterjee, H.D. Yang, S. Neeleshwar, Y.Y. Chen, Critical exponents of the $La_{0.7}Sr_{0.3}MnO_3$, $La_{0.7}Ca_{0.3}MnO_3$, and $Pr_{0.7}Ca_{0.3}MnO_3$ systems showing correlation between transport and magnetic properties. J. Appl. Phys. **98**(10), 103903 (2005)
6. F. Bern, M. Ziese, I. Vrejoiu, X. Li, P.A. van Aken, Magnetic and magnetotransport properties of ultrathin $LaBaMnO_3$ epitaxial films embedded in $SrRuO_3$. New J. Phys. **18**(5), 053021 (2016)
7. E. Brück, O. Tegus, X. Li, F.R. De Boer, K.H.J. Buschow, Magnetic refrigeration towards room-temperature applications. Phys. B **327**(2–4), 431–437 (2003)
8. A. Selmi, R. M'nassri, W. Cheikhrouhou-Koubaa, N.C. Boudjada, A. Cheikhrouhou, The effect of Co doping on the magnetic and magnetocaloric properties of $Pr_{0.7}Ca_{0.3}Mn_{1-x}Co_xO_3$ manganites. Ceram. Int. **41**(6), 7723–7728 (2015)
9. S.C. Maatar, R. M'nassri, W.C. Koubaa, M. Koubaa, A. Cheikhrouhou, Structural, magnetic and magnetocaloric properties of $La_{0.8}Ca_{0.2-x}Na_xMnO_3$ manganites ($0 \leq x \leq 02$). J. Solid State Chem. **225**, 83–88 (2015)
10. M.H. Phan, S.C. Yu, Review of the magnetocaloric effect in manganite materials. J. Magn. Magn. Mater. **308**(2), 325–340 (2007)
11. P. Lampen, A. Puri, M.H. Phan, H. Srikanth, Structure, magnetic, and magnetocaloric properties of amorphous and crystalline $La_{0.4}Ca_{0.6}MnO_{3+\delta}$ nanoparticles. J. Alloys Compd. **512**(1), 94–99 (2012)
12. S. Das, D. Dhak, M.S. Reis, V.S. Amaral, T.K. Dey, Room temperature giant magnetoimpedance in $La_{0.7}Ba_{0.15}Sr_{0.15}MnO_3$ compound. Mater. Chem. Phys. **120**(23), 468–471 (2010)
13. M.D. Daivajna, N. Kumar, V.P.S. Awana, B. Gahtori, J.B. Christopher, S.O. Manjunath, A. Rao, Electrical, magnetic and thermal properties of $Pr_{0.6-x}Bi_xSr_{0.4}MnO_3$ manganites. J. Alloys Compd. **588**, 406–412 (2014)
14. M. Oumezzine, S. Kallel, O. Pena, N. Kallel, T. Guizouarn, F. Gouttefangeas, M. Oumezzine, Correlation between structural, magnetic and electrical transport properties of barium vacancies in the $La_{0.67}Ba_{0.33-x}\square_xMnO_3$ ($x = 0$, 0.05, and 0.1) manganite. J. Alloys Compd. **582**, 640–646 (2014)
15. P. Bisht, A. Kumar, R.N. Mahato, Magnetic and magnetocaloric properties of the nanocrystalline $Pr_{0.7}Ba_{0.2}Ca_{0.1}MnO_3$ sample. AIP Adv. **11**(1), 015239 (2021)
16. C.R. Duarte de Freitas, M. Marques de Góis, R. Bezerra da Silva, J.A. Pereira da Costa, J.M. Soares, Mater. Res. **21**, 1–7 (2018)
17. W. Boujelben, M. Ellouze, A. Cheikh-Rouhou, J. Pierre, Q. Cai, W.B. Yelon, C. Dubourdieu, Neutron diffraction, NMR and magneto-transport properties in the $Pr_{0.7}Sr_{0.3}MnO_3$ perovskite manganite. Phys. Status **191**(1), 243–254 (2002)
18. M. Chakraborty, P. Pal, B.R. Sekhar, Solid State Commun. **145**, 197–200 (2008)
19. M. Ellouze, W. Boujelben, H. Fuess, Rietveld refinement X-ray powder data of $Pr_{0.7}Ba_{0.3}MnO_3$. Powder Diffr. **18**(1), 29–31 (2003)
20. M. Ellouze, W. Boujelben, A. Cheikhrouhou, H. Fuess, R. Madar, Vacancy effects on the crystallographic and magnetic properties in lacunar $Pr_{0.7}Ba_{0.3-x}MnO_3$ oxides. Solid State Commun. **124**(4), 125–130 (2002)
21. H. Rached, D. Rached, M. Rabah, R. Khenata, A.H. Reshak, Full-potential calculation of the structural, elastic, electronic and magnetic properties of $XFeO_3$ (X = Sr and Ba) perovskite. Phys. B **405**(17), 3515–3519 (2010)
22. D. Rached, M. Hichour, M. Rabah, S. Benalia, H. Rached, R. Khenata, Prediction study of the structural, elastic, electronic and optical properties of the antiperovskite $BiNBa_3$. Solid State Commun. **149**(45–46), 2002–2006 (2009)
23. H. Benmhidi, H. Rached, D. Rached, M. Benkabou, Ab initio study of electronic structure, elastic and transport properties of fluoroperovskite $LiBeF_3$. J. Electron. Mater. **46**, 2205–2210 (2017)
24. I. Bourachid, M. Caid, O. Cheref, D. Rached, H. Heireche, B. Abidri, N. Benkhettou, Insight into the structural, electronic, mechanical and optical properties of inorganic lead bromide perovskite $APbBr_3$ (A = Li, Na, K, Rb, and Cs). Comput. Condens. Matter **24**, e00478 (2020)
25. H. Rached, S. Bendaoudia, D. Rached, Investigation of Iron-based double perovskite oxides on the magnetic phase stability, mechanical, electronic and optical properties via first-principles calculation. Mater. Chem. Phys. **193**, 453–469 (2017)
26. S. Al-Qaisi, M. Mushtaq, S. Alomairy, T.V. Vu, H. Rached, B.U. Haq, M.S. Al-Buriahi, First-principles investigations of Na_2CuMCl_6 (M = Bi, Sb) double perovskite semiconductors: materials for green technology. Mater. Sci. Semicond. Process. **150**, 106947 (2022)
27. K. Schwarz, P. Blaha, G.K. Madsen, Electronic structure calculations of solids using the WIEN2k package for material sciences. Comput. Phys. Commun. **147**(1–2), 71–76 (2002)
28. G. Kadim, R. Masrour, A. Jabar, A comparative study between GGA, WC-GGA, TB-mBJ and GGA+ U approximations on magnetocaloric effect, electronic, optic and magnetic properties of $BaMnS_2$ compound: DFT calculations and Monte Carlo simulations. Phys. Scr. **96**(4), 045804 (2021)
29. G. Kadim, R. Masrour, Thermoelectric, magneto-optic properties and magnetocaloric effect of PbS doped with Mn^{2+} ions. J. Inorg. Organomet. Polym. Mater. (2023). https://doi.org/10.1007/s10904-023-02677-x
30. G. Kadim, R. Masrour, Density functional theory and Monte Carlo simulation insights into electronic structure and magnetic properties in HoSi and CeSi. Mater. Today Commun. **37**, 107176 (2023)
31. G. Kadim, R. Masrour, Effect of Zn-doping CdTe on the internal and external quantum efficiency: ab initio calculations. J. Korean Ceram. **60**(6), 896–904 (2023)
32. A. Jabar, R. Masrour, G. Kadim, M. Hamedoun, A. Hourmatallah, N. Benzakour, J. Kharbach, Intrinsic ferromagnetism in $CoBr_2$ nanolayers: a DFT+U and Monte Carlo study. Commun. Theor. Phys. **73**(11), 115702 (2021)
33. G.K. Madsen, D.J. Singh, BoltzTraP: a code for calculating band-structure dependent quantities. Comput. Phys. Commun. **175**(1), 67–71 (2006)

34. G. Kadim, R. Masrour, A. Jabar, Magnetocaloric, electronic, magnetic, optical and thermoelectric properties in antiferromagnetic semiconductor $GdCrO_3$: Monte Carlo simulation and density functional theory. J. Cryst. Growth **581**, 126509 (2022)
35. V. Franco, J.S. Blázquez, A. Conde, Field dependence of the magnetocaloric effect in materials with a second order phase transition: a master curve for the magnetic entropy change. Appl. Phys. Lett. **89**(22), 222512 (2006)
36. A.L. Lima, A.O. Tsokol, K.A. Gschneidner Jr., V.K. Pecharsky, T.A. Lograsso, D.L. Schlagel, Magnetic properties of single-crystal $DyAl_2$. Phys. Rev. B **72**(2), 024403 (2005)